Biosensors and Bioelectronics 142 (2019) 111475

Contents lists available at ScienceDirect

Biosensors and Bioelectronics

journal homepage: www.elsevier.com/locate/bios

Functionalized aptamer with an antiparallel G-quadruplex: Structural remodeling, recognition mechanism, and diagnostic applications targeting CTGF

Shunxiang Gao[b,c,d], Wei Hu[f], Xin Zheng[a,***], Sheng Cai[e,**], Jihong Wu[b,c,d,*]

[a] Department of Clinical Laboratory, Longhua Hospital, Shanghai University of Traditional Chinese Medicine, Shanghai, China
[b] Eye Institute, Eye and ENT Hospital, College of Medicine, Fudan University, Shanghai, China
[c] Shanghai Key Laboratory of Visual Impairment and Restoration, Science and Technology Commission of Shanghai Municipality, Shanghai, China
[d] Key Laboratory of Myopia (Fudan University), Chinese Academy of Medical Sciences, National Health Commission, Shanghai, China
[e] Institute of Drug Metabolism and Pharmaceutical Analysis, Zhejiang Province Key Laboratory of Anti-Cancer Drug Research, Zhejiang University, Hangzhou, China
[f] Chengdu FenDi Technology Co., Ltd., Chengdu, China

ARTICLE INFO

Keywords:
Aptamer
CTGF
Structural remodeling
Recognition mechanism
Enzyme-linked aptamer sandwich assay

ABSTRACT

Connective tissue growth factor (CTGF), a widely used biomarker, is involved in many diseases, such as diabetic retinopathy, diabetic nephropathy, and rheumatoid arthritis, and it is often over-expressed in human malignant tumors. Therefore, sensitive, specific and efficient detection methods for CTGF are needed for the early diagnosis and assessment of prognosis. In this study, an aptamer, APT1, that specifically binds to CTGF was obtained by SELEX technology. Circular dichroism spectroscopy indicated that APT1 formed interconvertible parallel and antiparallel G-quadruplexes. Mutation and truncation strategies optimized APT1 and improved its functions, yielding APT1M6T, which folded into an antiparallel G-quadruplex with higher targeting affinity. A stable APT1M6T-CTGF complex model was established by molecular simulation, which helped elucidate the molecular recognition mechanism of APT1M6T and CTGF and also provided experimental guidance for rational site-directed modification of APT1M6T. A locked nucleic acid sequence was then integrated into APT1M6T to generate APT1M6TL, which had higher structural stability. A BLI-based enzyme-linked aptamer sandwich assay (BLI-ELASA) was successfully developed. The method exhibited a broad detection range from 0.05 to 50 nM with a low detection limit of 0.02 nM. The method showed high selectivity, reproducibility, and stability for analysis of CTGF in spiked serum and urine samples. This developed BLI-ELASA is promising and enables real-time, sensitive and rapid detection of the disease-specific biomarker CTGF.

1. Introduction

Connective tissue growth factor (CTGF), also known as CCN2, is a highly conserved member of the CCN family of growth factors (Perbal, 2004). It plays an important role in many physiological and pathological activities, including angiogenesis, fibrosis, inflammation, wound healing, tumor metastasis, and deterioration (Battula et al., 2013; Mokalled et al., 2016). There is some evidence that CTGF is also involved in the pathogenesis and progression of diabetic eye diseases, and it may be a novel early diagnostic and potent therapeutic target for diabetic retinopathy (Klaassen et al., 2015). In diabetic nephropathy, CTGF as a progressive promoter is strongly overexpressed in glomeruli of diabetic patients with nephropathy, and its levels in urine and plasma correlate significantly with the progression of diabetic nephropathy (Roestenberg et al., 2004). Furthermore, serum CTGF levels are considered to be a highly discriminatory diagnostic indicator for fibrosis, malignant transformation, and rheumatoid arthritis (Gressner et al., 2013; Yang et al., 2017). Therefore, accurate, fast, and sensitive detection of CTGF as a disease-specific protein biomarker, especially in blood, urine, or other bodily fluids, is an important approach to achieve early diagnosis of diseases and monitor subsequent therapeutic treatments. To date, several immunological analytical methods, including

* Corresponding author. Eye Institute, Eye and ENT Hospital, College of Medicine, Fudan University, Shanghai 200032, China.
** Corresponding author. Institute of Drug Metabolism and Pharmaceutical Analysis, Zhejiang Province Key Laboratory of Anti-Cancer Drug Research, Zhejiang University, Hangzhou 310058, China.
*** Corresponding author. Department of Clinical Laboratory, Longhua Hospital, Shanghai University of Traditional Chinese Medicine, Shanghai 200032, China.
E-mail addresses: dearjanna@126.com (X. Zheng), caisheng@zju.edu.cn (S. Cai), jihongwu@fudan.edu.cn (J. Wu).

https://doi.org/10.1016/j.bios.2019.111475
Received 22 March 2019; Received in revised form 1 June 2019; Accepted 24 June 2019
Available online 02 July 2019
0956-5663/

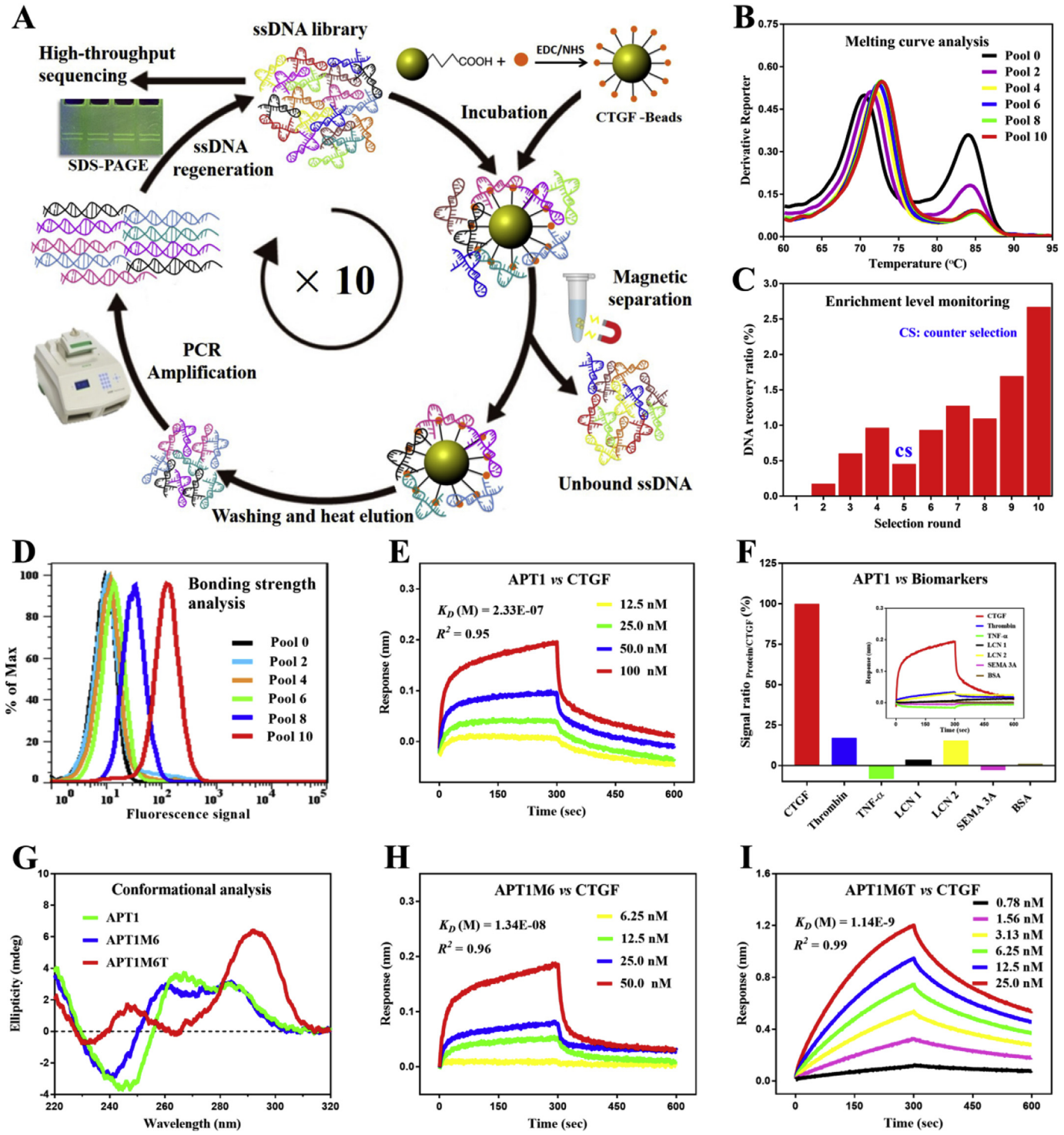

Fig. 1. Screening and optimization of CTGF-targeted aptamers. (**A**) Schematic diagram of the MB-SELEX. (**B**) Melting curve analysis of the enriched aptamer libraries by the QuantStudio Real-Time PCR System. (**C**) DNA recovery analysis of enriched aptamer libraries by Qubit 2.0 fluorometry. (**D**) Bonding fluorescence intensity analysis of the enriched aptamer libraries by flow cytometry. (**E**) Binding affinity analysis of the APT1 aptamer by BLI. (**F**) Binding specificity analysis of the APT1 aptamer. The binding signal was detected by BLI, and the relative signal strength of biomarkers was calculated by normalizing the CTGF signal to 100%. (**G**) Conformation analysis of the aptamers by circular dichroism. (**H**, **I**) Binding affinity analysis of optimized aptamers APT1M6 and APT1M6T by BLI.

ELISA, immunohistochemistry, and immunosensors, are mainly employed for CTGF detection (Bao et al., 2008; van Setten et al., 2016; Vorwerk et al., 2002). Although these immunological methods provide an invaluable insight into CTGF detection, they are usually costly, time-consuming, require well-trained personnel, and have limited applications. Antibodies are also used as molecular recognition agents, but their limited stability, complicated in vivo production, and typically undefined cross-reactivity are challenges to overcome. Therefore, significant efforts have been devoted to the development of novel alternatives that can replace antibodies for monitoring biomolecules, targeted drug delivery, and disease diagnosis and treatment.

Aptamers are functional ssDNA or RNA oligonucleotides that are folded into stable and unique three-dimensional structures through intramolecular interactions to perform their recognition, diagnostic and

therapeutic functions. They are generated by an in vitro selection technique termed "systematic evolution of ligands by exponential enrichment" (SELEX), and exhibit high selectivity and affinity for their targets (Ellington and Szostak, 1990; Teng et al., 2018; Tuerk and Gold, 1990). In addition, aptamers have significant advantages compared with antibodies, including precise preparation by the in vitro selection procedure without using experimental animals, easy achievement of chemical synthesis with very low cost, flexible labeling with various reporter molecules, and high stability under various conditions for long term storage and transportation (Groff et al., 2015). These properties make them popular in the various fields and have been widely used in development of various novel methods for diagnosis and targeted therapeutic agents (Gao et al., 2019; Ji et al., 2017; Meng et al., 2018; Tan et al., 2013; Zhou and Rossi, 2017; Zhou et al., 2016). Among them, aptasensors have become the fastest-growing detection platform by integration with biolayer interferometry (BLI), surface-enhanced Raman scattering, surface plasma resonance, and an electrochemical workstation (Famulok and Mayer, 2011; Gao et al. 2017, 2018). In particular, BLI is a promising sensor platform that can real-time, label-free, and automatically monitor the binding of target molecules to biorecognition molecules on inexpensive disposable fiber tips.

In this study, using SELEX technology, we successfully obtained a high-affinity aptamer, APT1, that specifically binds to CTGF. Mutation and truncation optimization strategies were introduced to further improve and regulate its functions and to produce an aptamer, APT1M6T, with higher targeting affinity, which consisted of only 21 core nucleotides, with an antiparallel G-quadruplex structure. To examine the recognition mechanism of APT1M6T and CTGF, we established a stable APT1M6T-CTGF complex model by molecular simulation. This not only theoretically explained the experimental results but also provided guidance for rational site-directed modification of the aptamer APT1M6T. The properties of the aptamer, including structural rigidity, thermal stability, and nuclease resistance, were further significantly improved by substitution and integration of locked nucleic acids (LNAs). Finally, these optimized aptamers were used to develop a BLI-based enzyme-linked aptamer sandwich assay (BLI-ELASA) for rapid, sensitive, and efficient detection of the disease-specific biomarker CTGF.

2. Materials and methods

All the materials, reagents, experimental methods and instrumentations used throughout this study are described in detail in the Supporting information.

3. Results

3.1. Selection and identification of CTGF aptamers

To obtain aptamers that bind to CTGF with high affinity and specificity, an ssDNA library consisting of 1×10^{15} random 40 nucleotide sequences was screened against CTGF beads by using an MB-SELEX procedure. The SELEX, which was carried out as described previously (Gao et al., 2016), is illustrated in Fig. 1A, and the following protocol is detailed in Table S1. To improve the screening efficiency, a counter selection step was introduced after the fourth round to eliminate ssDNA that nonspecifically bound to the bead matrix. Furthermore, free counter targets, including thrombin, TNF-α, LCN 1, LCN 2, and SEMA 3A, were gradually added to the positive incubation system to further improve the specificity of screening.

However, because enrichment of nonspecific ssDNA was unavoidable, further selection would not only unnecessarily consume extra resources and time but also make the selection prone to artifacts and even lead to failure of the experiment. Therefore, efficient monitoring of SELEX progression was essential for successful selection of aptamers. Here, we used a combined strategy of melting curve, pool recovery, and bonding strength analyses to monitor the convergence of aptamers during the screening process. As shown in Fig. 1B, the melting peaks shifted from the initial 70.5 °C to 72.8 °C and reached a plateau in the tenth round, indicating that the diversity of the library was reduced significantly. Simultaneously, the pool recovery rate was gradually increased with continuation of the SELEX procedure and reached a new plateau in the last round (Fig. 1C), which also showed significant enrichment of the screened library. To further evaluate the degree of enrichment for specific aptamers in pools, FAM-labeled ssDNA pools were incubated with CTGF beads for flow cytometric analysis. As shown in Fig. 1D, compared with the initial ssDNA library (Pool 0), increasing fluorescence intensities were observed as the screening progressed. Moreover, the fluorescence intensity of the tenth round was significantly higher than that of the eighth round, suggesting that more ssDNA bound to CTGF in the last round of the library. Therefore, the selection cycles were stopped, and Pool 10 was amplified for high-throughput sequencing (HTS).

Multiple sequence alignment of the top 30 most frequently found sequences identified by HTS were performed by Clustal X software (Fig. S1). We found that these sequences were highly consistent (differing by only a few base mutations). Therefore, the representative sequence of APT1 was chosen for further analysis of binding affinity and specificity for CTGF by BLI. As shown in Fig. 1E, CTGF at various concentrations (12.5, 25, 50, and 100 nM) was analyzed for association over 5 min and dissociation over 5 min. The results revealed that the APT1 interacted with CTGF with a high binding affinity (K_D = 233 nM). In addition, APT1 was exposed to other biomarkers, including thrombin, TNF-α, LCN 1, LCN 2, SEMA 3A, and BSA, and almost no binding signal was observed (Fig. 1F). These results indicated that we obtained a high-affinity aptamer, APT1, which specifically bound to CTGF.

3.2. Mutation and truncation optimization of the aptamer APT1

In addition to the selection process, mutation and truncation strategies were employed for optimization of the aptamer APT1 to further improve and regulate its functions. Based on QGRS Mapper predictions (Kikin et al., 2006), we found that APT1 formed G-quadruplex structures. Circular dichroism (CD) spectroscopy showed that the APT1 might form a parallel G-quadruplex structure with a characteristic positive peak at 265 nm and negative peak at 245 nm, whereas along with the other positive peak at 285 nm, it might also form an antiparallel G-quadruplex structure (Fig. 1G). To ensure that the aptamer tended to fold into a single and stable G-quadruplex structure, a rational site-directed mutagenesis optimization strategy was first applied to the sequence of APT1. Prediction by QGRS Mapper revealed that APT1-M1–APT1M8 folded into a G-quadruplex that may have higher structural stability (Table S2). The binding experiments revealed that only APT1M6 exhibited higher binding affinity to CTGF (K_D = 13.4 nM, Fig. 1H), whereas APT1M2 and APT1M3 showed almost no change, and other sequences exhibited a significant reduction. In addition, compared with the CD spectrum of APT1, the characteristic absorption peak of the APT1M6 aptamer showed a blue shift according to the positive peak at 260 nm and negative peak at 240 nm (Fig. 1G). Therefore, we suspected that it may be due to conversion of the aptamer APT1M6 to an antiparallel G-quadruplex structure or an increased proportion of folded antiparallel G-quadruplex structures, leading to significant improvement of binding affinity.

To test our hypothesis, nucleotides at both ends of the APT1M6 sequence were truncated based on QGRS Mapper predictions (Table S2). As shown in Fig. 1G, the CD spectrum of the truncated APT1M6T displayed two characteristic positive bands at 295 and 245 nm and a negative band at 230 nm, indicating that the aptamer APT1M6T had completely folded into an antiparallel G-quadruplex structure. Furthermore, our data showed stronger binding affinity (K_D = 1.14 nM) between APT1M6T and CTGF (Fig. 1I). These results indicated that the APT1M6T with an antiparallel G-quadruplex structure had improved target affinity, whereas truncation at both ends of APT1M6 caused

folding into a parallel G-quadruplex structure with a significant reduction in binding affinity, which may have been due to steric hindrance. Thus, we obtained a higher targeting affinity aptamer, APT1M6T, with an antiparallel G-quadruplex structure, which consisted of only 21 core nucleotides.

3.3. Determination of the target CTGF-binding region

To analyze the interactions of APT1M6T and CTGF, the binding region of CTGF was determined. As shown in Fig. S2A, the N-terminal, middle, and C-terminal regions of CTGF respectively interacted with APT1M6T. Both the C-terminal (K_D = 3.9 nM) and middle (K_D = 86.1 nM) regions of CTGF bound to APT1M6T and showed good binding affinity. Only the N-terminal region of CTGF exhibit no binding, which may be because the N-terminal region was immobilized on the bead surface in SELEX, resulting in a relatively low probability of collision and binding with aptamers. The interaction analyses suggested that full-length CTGF may simultaneously bind two molecules of APT1M6T at different domains. To test this hypothesis, an ELASA was integrated into the BLI system. As shown in Fig. S2B, the APT1M6T aptasensor was used to capture free target protein in buffer, followed by incubation with HRP-labeled APT1M6T and signal amplification using a DAB solution. Only full-length CTGF produced a dramatic signal, whereas different regions of CTGF showed no change in response. These results indicated formation of a sandwich structure complex consisting of biotin-labeled APT1M6T, full-length CTGF, and HRP-labeled APT1M6T. Therefore, we obtained the optimal aptamer APT1M6T that simultaneously bound to two different domains of CTGF.

3.4. Analysis of the binding mechanism between APT1M6T and CTGF

To further examine the recognition mechanism of APT1M6T and CTGF, we designed a series of molecular modeling, docking, and dynamics simulation experiments. As shown in Fig. 2A, APT1M6T contained three G-tetrads and folded into an antiparallel G-quadruplex structure, which was consistent with the experimental results. The structures “ATA” and “TAT” repeatedly opened as a binding pocket that specifically bound CTGF and formed a stable complex. Furthermore, the “TTT” structure acted as a linker connecting three G-tetrads and might play an important role in stabilizing the entire G-quadruplex structure. The optimized CTGF structure is shown in Fig. 2B. CTGF mainly consists of β-sheets and forms a long ribbon structure, and the N- and C-terminals are in the middle of ribbon. To investigate the binding mode of APT1M6T to CTGF, two APT1M6T molecules were docked successively to CTGF, and the appropriate conformations were selected according to the ZDOCK score. The first docked APT1M6T was named G-quadruplex 1 with a ZDOCK score of 1401.68, and the second docked ligand was named G-quadruplex 2 with a ZDOCK score of 1000.99.

To further assess the structural stability of the complex in an aqueous solution, a 40 ns molecular dynamics (MD) simulation was performed. Root mean square deviation (RMSD), describing the deviation of a system relative to the initial structure is a significant parameter to evaluate the convergence of a system. Fig. 3A shows the RMSD variation of the complex. After 30 ns, ATP1M6T-CTGF tended to be stable in the aqueous solution with an RMSD value of 0.78 ± 0.07 nm. Radius of gyration (Rg) is an important parameter to evaluate stability, which indicates the size of a complex. As shown in Fig. 3B, the Rg of ATP1M6T and CTGF was essentially stable with a value of 2.97 ± 0.06 nm after 30 ns, indicating that the complex conformation had not significantly changed. Both RMSD and Rg suggested that APT1M6T can be stably combined with CTGF at a ratio of 2:1 after rapid structural adjustment. Fig. 3C shows five fragments of trajectory during a 40 ns simulation to further characterize the conformational fluctuations of the ATP1M6T-CTGF complex. No obvious conformational changes occurred during the simulation, and two APT1M6T molecules stably bound to both ends of the CTGF long ribbon. The conformation analysis also showed that

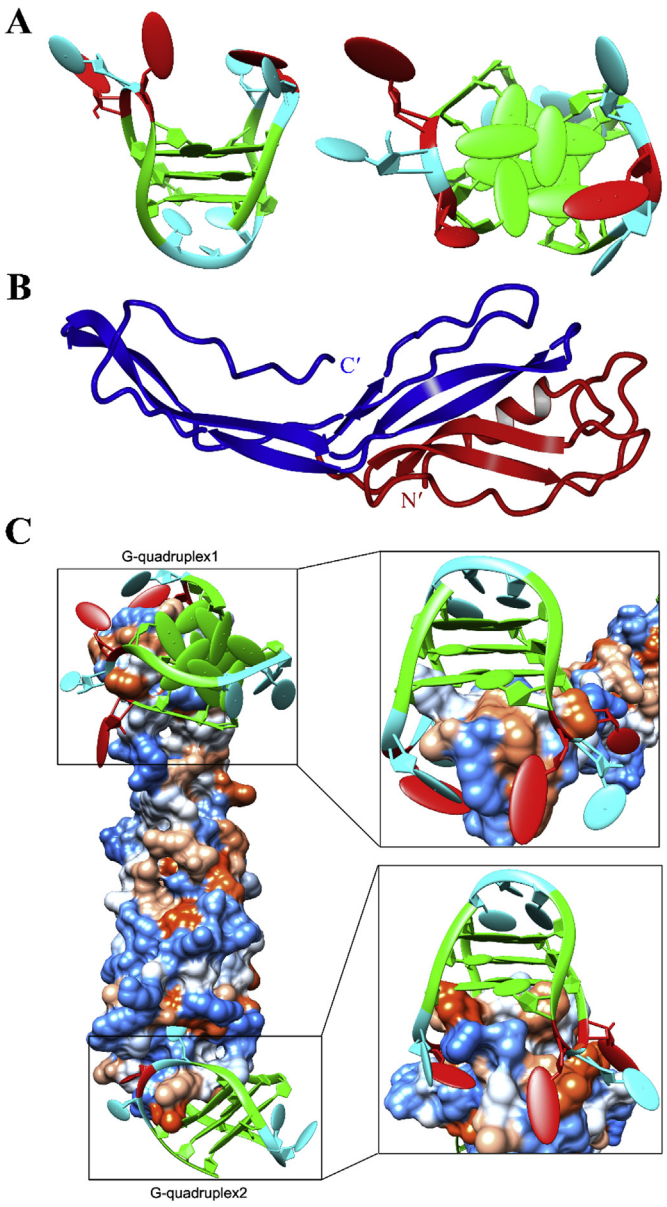

Fig. 2. Molecular modeling and docking. (**A**) Three-dimensional structure of APT1M6T. Front view (left) and vertical view (right). Red, green, and blue represent adenine, guanine, and thymine, respectively. (**B**) Structure of CTGF. Red and blue indicate the middle and C-terminal regions, respectively. (**C**) ATP1M6T-CTGF complex structure. Orange indicates the hydrophobic area and blue indicates the hydrophilic area. (For interpretation of the references to colour in this figure legend, the reader is referred to the Web version of this article.)

APT1M6T bound to CTGF at a ratio of 2:1. Specifically, G-quadruplex 1 bound to the C-terminal region, whereas G-quadruplex 2 mainly bound to the middle region of CTGF and interacted with the C-terminal region.

To further uncover the recognition mechanism of APT1M6T for CTGF, hydrogen bonds and hydrophobic, π-π, and cation-π interactions during the 40 ns MD simulation were analyzed. The numbers of hydrogen bonds (Fig. 3D) and hydrophobic interactions (Fig. 3E) in the two complex systems were stable after 30 ns with four and eight, respectively. These stable interactions enhanced the binding affinity between APT1M6T and CTGF. Because all of the bases in the G-quadruplex are aromatic rings, there may be corresponding π-π and cation-π interactions. The cation-π interactions of CTGF with G-quadruplexes 1 and 2 were both one (Fig. 3G), while the number of π-π interactions of

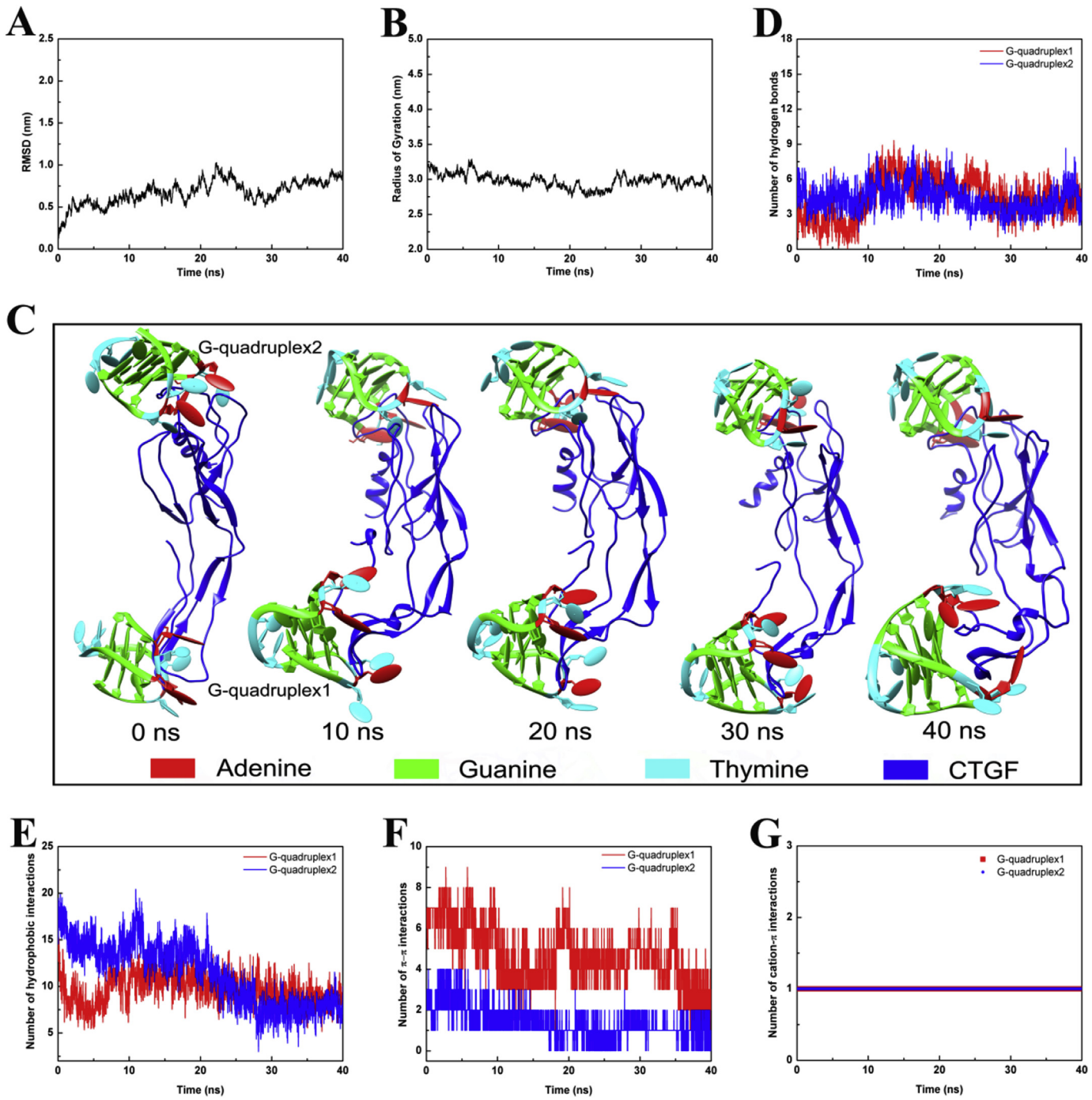

Fig. 3. Molecular dynamics simulations. RMSD of Cα atoms (**A**) and Rg (**B**) of the CTGF-APT1M6T complex versus simulation time. (**C**) Conformations of the complex during molecular dynamics simulation. The number of hydrogen bonds (**D**), hydrophobic interactions (**E**), π-π interactions (**F**), and cation-π interactions (**G**) between G-quadruplexes and CTGF versus simulation time.

G-quadruplex 1 was more than that of G-quadruplex 2 (Fig. 3F). To further identify key amino acids or bases in the binding mechanism, analysis of the structure after 40 ns of MD simulation was performed. The results shows that the bases in G-quadruplexes 1 and 2 involved in the interactions were mainly distributed in the "TAT", "ATA", and G-tetrad (G3, G7, G15, and G19) structures near CTGF (Table S3), indicating that these residues play a key role in the recognition of CTGF by APT1M6T. "TAT" and "ATA" structures participated in hydrogen bonds and hydrophobic interactions, while the G-tetrad structure contributed to hydrophobic and π-π interactions. Specifically, the hydroxyl group and benzene ring of Tyr279 in CTGF formed a hydrogen bond, and hydrophobic and π-π interactions with several bases in G-quadruplex 1, confirming that Tyr279 was the key residue in G-quadruplex 1 binding. Moreover, Asn198, Met194, Ile195, and Phe188 in CTGF, which constituted the binding site, formed hydrogen bonds and hydrophobic and π-π interactions with G-quadruplex 2. In general, the strong interaction between APT1M6T and CTGF was an important factor for high affinity and stable binding, and the hydrogen bonding and hydrophobic and π-π interactions in the complex were particularly critical.

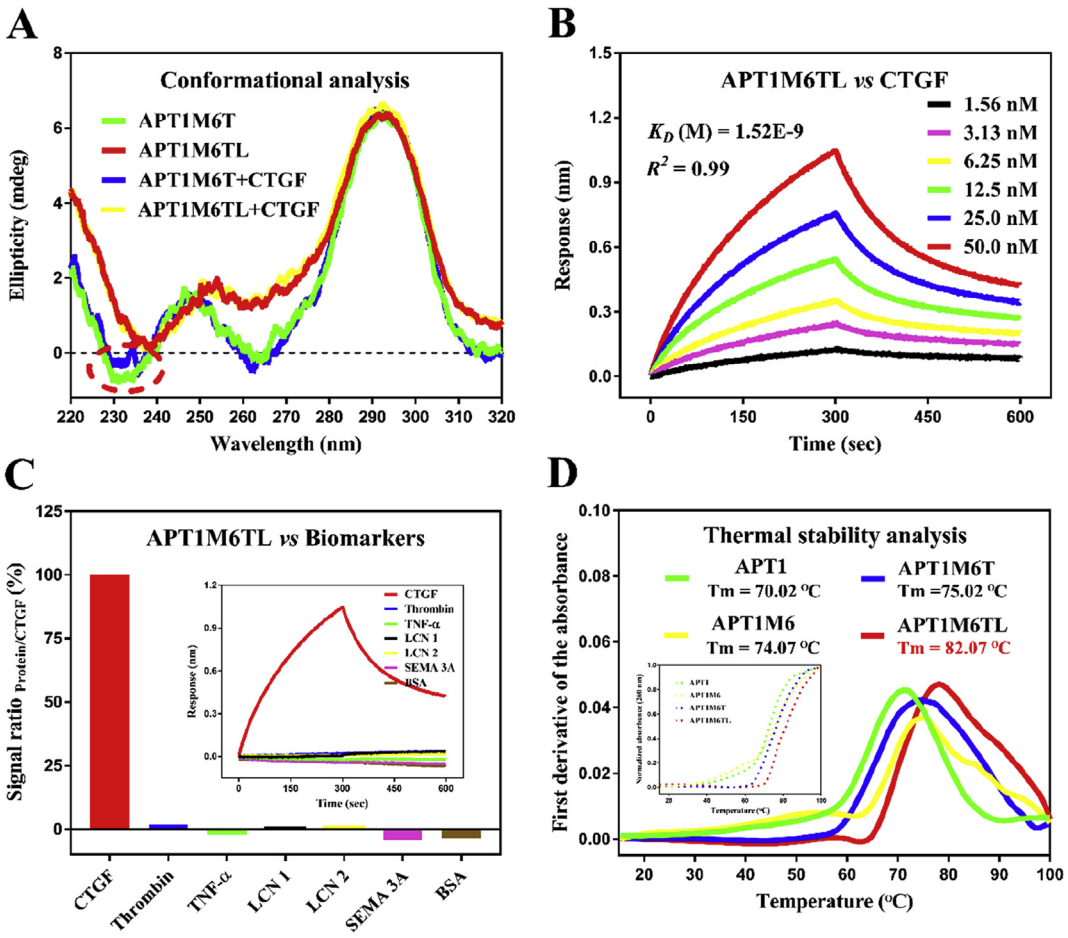

Fig. 4. LNAs-stabilized aptamer APT1M6TL. (**A**) Conformation analysis of the aptamers. CD spectra of 1 μM aptamers in binding buffer before (green and red) and after (blue and yellow) binding to 2 μM CTGF. (**B**) Binding affinity analysis of APT1M6TL and CTGF. (**C**) Binding specificity analysis of APT1M6TL. (**D**) Thermal stability analysis of the aptamers. Melting profiles were normalized by absorbance at 15 and 100 °C, and the first derivatives of the absorbance are shown. (For interpretation of the references to colour in this figure legend, the reader is referred to the Web version of this article.)

3.5. LNA incorporation into APT1M6TL and its stability improvement

Based on the analyses of aptamer structures and the binding mechanism of APT1M6T and CTGF, LNAs were integrated into the APT1M6TL sequence (Table S2) to improve its performance. Although the absorption peak of APT1M6TL was red shifted based on the positive peak at 255 nm and negative peak at 238 nm, APT1M6TL still folded into an antiparallel G-quadruplex structure and maintained high affinity and specificity for binding to CTGF (Fig. 4A, 4B and 4C). In addition, when CTGF bound to APT1M6T, it induced slight changes in the intensity of the aptamer's characteristic absorption peak at 230 nm. However, when combined with APT1M6TL, the CD spectrum of the aptamer was almost unchanged, indicating improvement in the structural rigidity of the aptamer modified by the LNAs. Therefore, the stability of APT1M6TL binding to CTGF was further improved, which would facilitate its biological functions for recognition, diagnosis, and treatment.

Subsequently, the thermal stabilities of aptamers were measured (Fig. 4D). Although the original APT1 aptamer exhibited high thermal stability (Tm = 70.02 °C), the site mutation strategy increased the Tm value of the APT1M6 aptamer (Tm = 74.07 °C) by 4.05 °C. Furthermore, the stability of APT1M6TL was further improved (Tm = 82.07 °C) when the LNAs were introduced into the APT1M6T sequence, although the truncated APT1M6T aptamer showed similar thermal stability to APT1M6. More importantly, the higher Tm indicated that these aptamers maintained their structure more persistently at around 37 °C.

Finally, we examined the resistance of the aptamers to nuclease digestion in 97% human serum at 37 °C for up to 72 h. As shown in Fig. S3, although the original APT1 aptamer exhibited high nuclease resistance and a small amount of aptamer remained at 24 h, mutation and truncation optimization increased APT1M6T aptamer resistance in human serum until 48 h. In addition, incorporation of LNAs into the aptamer structure blocked the endonuclease activity, thus a large amount of the APT1M6TL aptamer was not degraded at 72 h in 97% human serum. In general, with the application of a series of optimizations, including site mutations, sequence truncation, and LNAs replacement, the binding affinity, targeting specificity, structural rigidity, thermal stability, and nuclease resistance of aptamers were improved significantly.

3.6. Setup and optimization of the BLI-ELASA

To enable rapid and effective monitoring of CTGF, we developed a BLI-ELASA. As outlined in Fig. 5A, in the first step of the assay, APT1M6TL-labeled aptasensors were baselined in binding buffer for 1 min, followed by 5 min of incubation with the samples to capture free CTGF. After a 0.5 min wash step, the biosensors were then submerged for another 3 min in a well containing HRP-labeled APT1M6T aptamers to form a sandwich structure consisting of a APT1M6TL:CTGF:HRP-labeled APT1M6T complex, followed by a another 0.5 min wash step. Finally, the biosensors were submerged in HRP substrate solution for 5 min, resulting in the formation of non-soluble substrate crystals that precipitated on the biosensor surface, which caused a large change in

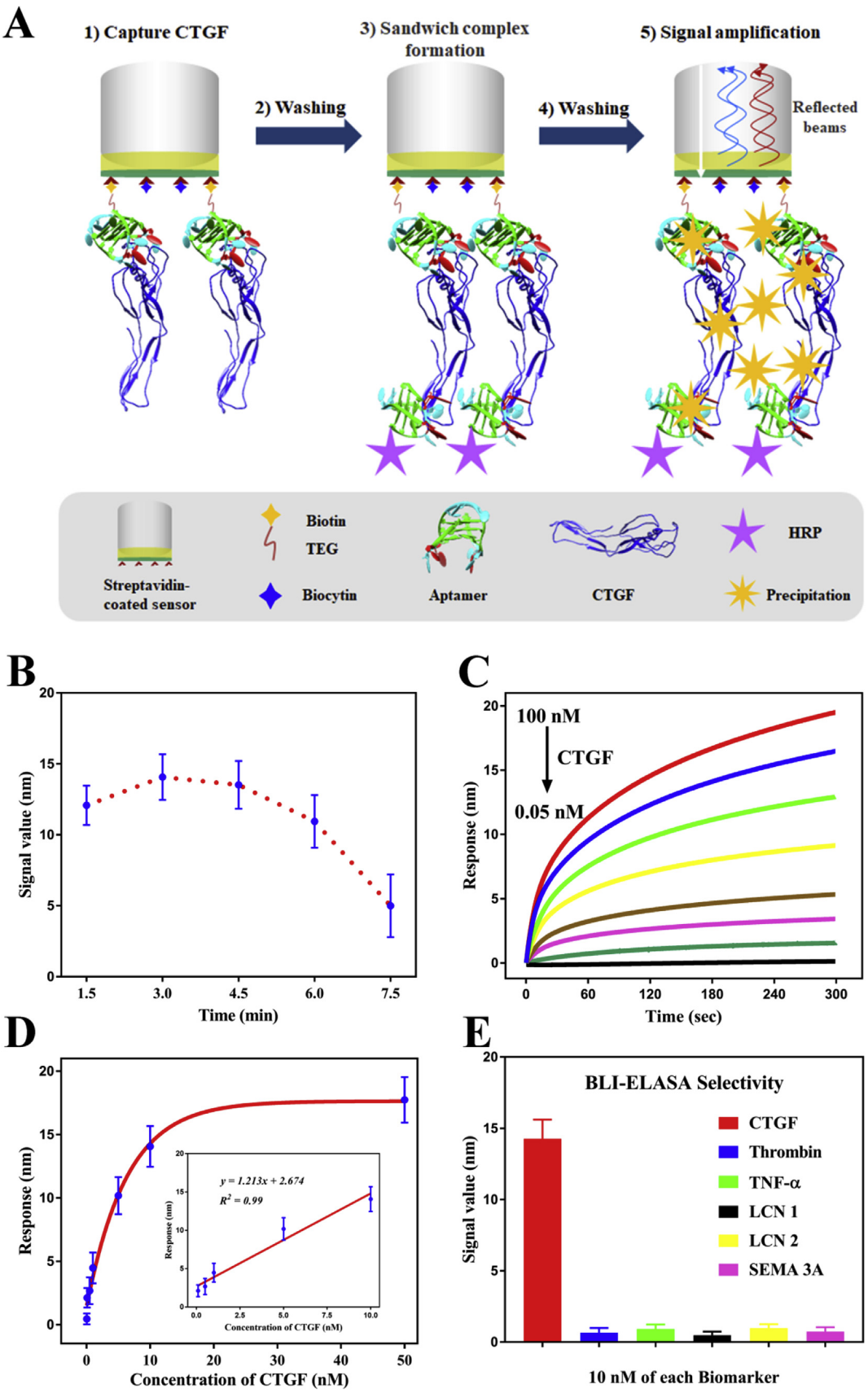

Fig. 5. BLI-ELASA detection system. (**A**) Schematic representation of the BLI-ELASA. (**B**) Optimization of incubation time for HRP-labeled APT1M6T. (**C**) Response plot for the BLI-ELASA after addition of CTGF at various concentrations. The response was recorded at the last step of the assay. (**D**) Calibration curve for CTGF, plot of response *vs* CTGF concentration, in the range of 0.05–50 nM. (**E**) Selectivity of the BLI-ELASA for various biomarkers. Error bars represent the standard deviation of measurements.

Table 1
Analysis of CTGF in serum and urine samples by the BLI-ELASA.

Samples	Spiked (nM)	Recovery (%)	CV (%)
Serum	1	106.38	19.83
	5	112.05	11.97
	25	116.91	6.55
Urine	1	103.25	12.66
	5	106.49	8.11
	25	107.76	5.58

the optical thickness of the biosensor layer and thus induced a significant spectral shift and amplified the detection signal. Therefore, even if the CTGF level in samples is very low, which usually does not induce a significant interference shift, it can be detected by the last step to enhance the signal.

Detection sensitivity can be greatly improved using a BLI-ELASA. However, the HRP-labeled APT1M6T aptamer, which was used to form the sandwich complex and amplify the detection signal, is a key factor in this assay. Theoretically, higher concentrations of the HRP-labeled aptamer will lead to decreased sensitivity (competitive dissociation of more target proteins) and lower concentrations will result in a reduced signal (incomplete formation of the sandwich complex on the biosensor layer). Therefore, the concentration effect of HRP-labeled APT1M6T was analyzed, and the signal was increased with increasing HRP-labeled aptamer concentrations up to 100 nM (data not shown). Therefore, a concentration of 100 nM HRP-labeled APT1M6T was selected to balance signal strength and accuracy of the BLI-ELASA system. In addition, it is crucial that the biosensor specifically binds free HRP-labeled aptamer to form the equilibrium detection system without disturbing the APT1M6TL: CTGF:HRP-labeled APT1M6T complex. Generally, a longer contact time allows more of the free HRP-labeled APT1M6T to be captured for stronger signals. However, as more HRP-labeled aptamer is depleted from the solution over time, the sandwich complex may dissociate, disrupting the equilibrium and altering the signal value. To evaluate this effect, contact times from 1.5 to 7.5 min were assessed, and the signal was increased with increasing HRP-labeled aptamer incubation times up to 3 min (Fig. 5B), after which a significant reduction occurred. This may be because the detection probe was dissociated when the incubation time was greater than 4.5 min, resulting in a significant decrease in signal value. Therefore, to stabilize the detection system, a contact time of 3 min was selected.

3.7. BLI-ELASA for CTGF detection

To further examine detection of CTGF using the BLI-ELASA, time-dependent changes in signals of CTGF at various concentrations were investigated under the optimal experimental conditions. As shown in Fig. 5C, the signal of the BLI-ELASA was increased by increasing the concentration of CTGF. A calibration curve of the signal value against the concentration range from 0.05 to 50 nM CTGF was obtained (Fig. 5D), and then fitted to the following sigmoidal logistic four-parameter equation:

$$y = (R_{max} - R_{min}) / [1 + (x/EC50)^{b}] + R_{min} \quad (1)$$

Here, R_{max} and R_{min} are the maximum and minimum signal values, respectively, and b is the slope of the curve. $EC50$ is the CTGF concentration leading to 50% of the maximum response. After generation of the experimental data, the following equation was obtained:

$$y = (19.39782 - 0.9485) / [1 + (x/4.53497)^{-0.99627}] + 0.9485 \quad R^2 = 0.99 \quad (2)$$

Moreover, the BLI-ELASA exhibited a good linear detection range from 0.1 to 10 nM CTGF, which can be represented by the linear regression equation:

$$y = 1.213x + 2.674 \quad R^2 = 0.99 \quad (3)$$

The limit of detection (LOD) of the BLI-ELASA for CTGF quantification was calculated to be 0.02 nM (S/N = 3), where the noise level was the standard deviation of multiple measurements of blank samples. A cross reactivity experiment with thrombin, TNF-α, LCN 1, LCN 2, and SEMA 3A was further performed, and no significant response was obtained with all non-targeted biomarkers (Fig. 5E). The developed BLI-ELASA showed good analytical performance for detection of CTGF, and the LOD was comparable, being at a picomolar level of the reported ELISA, which is the gold standard for CTGF detection (Bao et al., 2008). Furthermore, measurement of CTGF using the ELISA took at least 2 h, whereas the detection steps in the BLI-ELASA were completed in just 15 min. Most importantly, the developed BLI-ELASA detection system relies mainly on the principle of BLI, and it could achieve real-time, automatic, high-throughput monitoring of CTGF.

3.8. Analysis of CTGF in clinical samples

To validate the actual effectiveness of the developed BLI-ELASA, free CTGF was spiked into clinical serum and urine samples, which had been diluted 10-fold using binding buffer, at final concentrations of 1, 5, and 25 nM, and analyzed using the preset calibration curve. As shown in Table 1, good recovery percentages of 103.25% to 116.91% were obtained, indicating no significant interference of the BLI-ELASA signal by the clinical serum and urine samples. The coefficient of variation (5.58% to 19.83%) was acceptable, indicating high repeatability and stability of the proposed method. These results confirmed that the developed BLI-ELASA had would be applicable to clinical sample analysis.

4. Discussion

Accurate, fast, and sensitive detection of the disease-specific biomarker CTGF, especially in blood, urine, or other bodily fluids, is an important approach to achieve early disease diagnosis and monitor subsequent therapeutic treatments. In this study, the high-affinity aptamer APT1 that specifically bound to CTGF was obtained by SELEX technology. To improve the success rate of SELEX, we developed a combined strategy of melting curve, pool recovery, and bonding strength analyses to monitor the convergence of aptamers in the screening process. Although primary aptamers can be obtained by SELEX, they are usually unsuitable for direct clinical or even laboratory applications. To further improve and regulate its functions, mutation and truncation strategies were used to optimize APT1. The core sequence of the aptamer with an antiparallel G-quadruplex structure was then obtained, which included only 21 nucleotides. In addition, compared with the original APT1, the binding affinity between the optimized APT1M6T aptamer and CTGF was increased by about 200-fold. More importantly, APT1M6T simultaneously bound to two different domains of CTGF, which is significant for the design of novel detection schemes and development of targeted drug delivery systems, as well as for the research and development of nucleic acid drugs.

To further examine the recognition mechanism of APT1M6T and CTGF, we applied a molecular simulation to predict the structure of APT1M6T, CTGF, and their binding complex. The results showed that APT1M6T folded into an antiparallel G-quadruplex structure with three G-tetrads and bound to CTGF at a ratio of 2:1, mainly through many hydrogen bonds, and hydrophobic and π-π interactions. The interaction analysis results showed that G-quadruplex 1 only interacted with the C-terminal region (A244–D347) of CTGF, whereas G-quadruplex 2 not only had a major interaction with the middle region of CTGF (Q172-E243) but also certain interactions with C-terminal regions (e.g., Cys256, Arg258, and Pro308). Such binding may explain why APT1M6T bound to the C-terminal region of CTGF with higher affinity than that for the middle region alone. Overall, we established a stable

and reliable APT1M6T-CTGF complex model, which theoretically explained the experimental results and the molecular binding mechanism of APT1M6T and CTGF.

Based on the analysis of the interaction between APT1M6T and CTGF, instead of direct sites for targeted binding, we found that the "TTT" structure acted as an intermediate link connecting three G-tetrads to form an antiparallel G-quadruplex structure. Therefore, LNAs were integrated into APT1M6TL and maintained high affinity and specificity for CTGF. More importantly, the CD spectrum demonstrated that the LNA-modified APT1M6TL aptamer appeared to fold into an antiparallel G-quadruplex structure with relatively high rigidity. In addition, the Tm value of the LNA-modified APT1M6TL was further increased to 82.07 ˚C and a large amount of the APT1M6TL was not degraded at 72 h in 97% human serum. Therefore, by using a series of optimization strategies, we were able to significantly improve the key functions and properties of aptamers, including binding affinity, targeting specificity, structural rigidity, thermal stability, and nuclease resistance.

To achieve rapid and effective monitoring of target protein, the aptamer as a capture probe was immobilized on an SA sensor to detect CTGF by the BLI system. Although BLI enables automated, label-free, real-time, and high-throughput detection of targets that bind to aptasensors, only high concentrations of CTGF can be detected effectively. Because CTGF bound to two molecules of the aptamer, the optimized aptamer could be used as capture and detection probes simultaneously. To significantly improve the detection sensitivity, we coupled the advantages of the BLI system with a signal enhancement step and developed a BLI-ELASA to detect CTGF. Furthermore, considering the balance between clinical application and detection costs, the LNA-modified APT1M6TL with high structural stability was used as a capture probe, and the HRP-labeled APT1M6T was used as a detection probe. The BLI-ELASA exhibited a broad detection range from 0.05 to 50 nM with a low LOD of 0.02 nM, and it showed good reproducibility and stability for analysis of clinical spiked serum and urine samples. Therefore, the developed BLI-ELASA is promising and enables real-time, rapid, sensitive and efficient detection of the disease-specific biomarker CTGF.

In conclusion, this work shows the selection, optimization, and binding mechanism of aptamers against CTGF and their application in a BLI biosensing platform.

Declaration of interests

The authors declare that they have no known competing financial interests or personal relationships that could have appeared to influence the work reported in this paper.

CRediT authorship contribution statement

Shunxiang Gao: Conceptualization, Writing - original draft, Formal analysis, Funding acquisition. **Wei Hu:** Software, Formal analysis. **Xin Zheng:** Conceptualization, Data curation, Funding acquisition. **Sheng Cai:** Conceptualization, Visualization. **Jihong Wu:** Conceptualization, Writing - review & editing, Funding acquisition.

Acknowledgements

This work was supported by the National Natural Science Foundation of China (81700883, 81702094, 81770925 and 81790641) and Science and Technology Commission of Shanghai Municipality (19ZR1471900, 17411971700). We appreciate Wenyi Du for his help and support in molecular simulation part.

Appendix A. Supplementary data

Supplementary data to this article can be found online at https://doi.org/10.1016/j.bios.2019.111475.

References

Bao, J., Tu, Z., Wang, J., Ye, F., Sun, H., Qin, M., Shi, Y., Bu, H., Li, Y.P., 2008. A novel accurate rapid ELISA for detection of urinary connective tissue growth factor, a biomarker of chronic allograft nephropathy. Transplant. Proc. 40 (7), 2361–2364.
Battula, V.L., Chen, Y., Cabreira Mda, G., Ruvolo, V., Wang, Z., Ma, W., Konoplev, S., Shpall, E., Lyons, K., Strunk, D., Bueso-Ramos, C., Davis, R.E., Konopleva, M., Andreeff, M., 2013. Connective tissue growth factor regulates adipocyte differentiation of mesenchymal stromal cells and facilitates leukemia bone marrow engraftment. Blood 122 (3), 357–366.
Ellington, A.D., Szostak, J.W., 1990. In vitro selection of RNA molecules that bind specific ligands. Nature 346 (6287), 818–822.
Famulok, M., Mayer, G., 2011. Aptamer modules as sensors and detectors. Acc. Chem. Res. 44 (12), 1349–1358.
Gao, S., Hu, B., Zheng, X., Cao, Y., Liu, D., Sun, M., Jiao, B., Wang, L., 2016. Gonyautoxin 1/4 aptamers with high-affinity and high-specificity: from efficient selection to aptasensor application. Biosens. Bioelectron. 79, 938–944.
Gao, S., Zheng, X., Hu, B., Sun, M., Wu, J., Jiao, B., Wang, L., 2017. Enzyme-linked, aptamer-based, competitive biolayer interferometry biosensor for palytoxin. Biosens. Bioelectron. 89 (Pt 2), 952–958.
Gao, S., Zheng, X., Wu, J., 2018. A biolayer interferometry-based enzyme-linked aptamer sorbent assay for real-time and highly sensitive detection of PDGF-BB. Biosens. Bioelectron. 102, 57–62.
Gao, S.X., Zheng, X., Tang, Y., Cheng, Y.J., Hu, X.B., Wu, J.H., 2019. Development of a fluorescently labeled aptamer structure-switching assay for sensitive and rapid detection of gliotoxin. Anal. Chem. 91 (2), 1610–1618.
Gressner, O.A., Fang, M., Li, H., Lu, L.G., Gressner, A.M., Gao, C.F., 2013. Connective tissue growth factor (CTGF/CCN2) in serum is an indicator of fibrogenic progression and malignant transformation in patients with chronic hepatitis B infection. Clin. Chim. Acta 421, 126–131.
Groff, K., Brown, J., Clippinger, A.J., 2015. Modern affinity reagents: recombinant antibodies and aptamers. Biotechnol. Adv. 33 (8), 1787–1798.
Ji, D., Wang, H., Ge, J., Zhang, L., Li, J., Bai, D., Chen, J., Li, Z., 2017. Label-free and rapid detection of ATP based on structure switching of aptamers. Anal. Biochem. 526, 22–28.
Kikin, O., D'Antonio, L., Bagga, P.S., 2006. QGRS Mapper: a web-based server for predicting G-quadruplexes in nucleotide sequences. Nucleic Acids Res. 34 (Web Server issue), W676-682.
Klaassen, I., van Geest, R.J., Kuiper, E.J., van Noorden, C.J., Schlingemann, R.O., 2015. The role of CTGF in diabetic retinopathy. Exp. Eye Res. 133, 37–48.
Meng, H.M., Hu, X.X., Kong, G.Z., Yang, C., Fu, T., Li, Z.H., Zhang, X.B., 2018. Aptamer-functionalized nanoscale metal-organic frameworks for targeted photodynamic therapy. Theranostics 8 (16), 4332–4344.
Mokalled, M.H., Patra, C., Dickson, A.L., Endo, T., Stainier, D.Y., Poss, K.D., 2016. Injury-induced ctgfa directs glial bridging and spinal cord regeneration in zebrafish. Science 354 (6312), 630–634.
Perbal, B., 2004. CCN proteins: multifunctional signalling regulators. Lancet 363 (9402), 62–64.
Roestenberg, P., van Nieuwenhoven, F.A., Wieten, L., Boer, P., Diekman, T., Tiller, A.M., Wiersinga, W.M., Oliver, N., Usinger, W., Weitz, S., Schlingemann, R.O., Goldschmeding, R., 2004. Connective tissue growth factor is increased in plasma of type 1 diabetic patients with nephropathy. Diabetes Care 27 (5), 1164–1170.
Tan, W., Donovan, M.J., Jiang, J., 2013. Aptamers from cell-based selection for bioanalytical applications. Chem. Rev. 113 (4), 2842–2862.
Teng, I.T., Li, X., Yadikar, H.A., Yang, Z., Li, L., Lyu, Y., Pan, X., Wang, K.K., Tan, W., 2018. Identification and characterization of DNA aptamers specific for phosphorylation epitopes of tau protein. J. Am. Chem. Soc. 140 (43), 14314–14323.
Tuerk, C., Gold, L., 1990. Systematic evolution of ligands by exponential enrichment: RNA ligands to bacteriophage T4 DNA polymerase. Science 249 (4968), 505–510.
van Setten, G.B., Trost, A., Schrodl, F., Kaser-Eichberger, A., Bogner, B., van Setten, M., Heindl, L.M., Grabner, G., Reitsamer, H.A., 2016. Immunohistochemical detection of CTGF in the human eye. Curr. Eye Res. 41 (12), 1571–1579.
Vorwerk, P., Hohmann, B., Oh, Y., Rosenfeld, R.G., Shymko, R.M., 2002. Binding properties of insulin-like growth factor binding protein-3 (IGFBP-3), IGFBP-3 N- and C-terminal fragments, and structurally related proteins mac25 and connective tissue growth factor measured using a biosensor. Endocrinology 143 (5), 1677–1685.
Yang, X.Y., Lin, K., Ni, S.M., Wang, J.M., Tian, Q.Q., Chen, H.J., Brown, M.A., Zheng, K.D., Zhai, W.T., Sun, L., Jin, S.W., Wang, J.G., 2017. Serum connective tissue growth factor is a highly discriminatory biomarker for the diagnosis of rheumatoid arthritis. Arthritis Res. Ther. 19.
Zhou, J.H., Rossi, J., 2017. Aptamers as targeted therapeutics: current potential and challenges. Nat. Rev. Drug Discov. 16 (3), 181–202.
Zhou, S.S., Zhang, L., Cai, Q.Y., Dong, Z.Z., Geng, X., Ge, J., Li, Z.H., 2016. A facile label-free aptasensor for detecting ATP based on fluorescence enhancement of poly(thymine)-templated copper nanoparticles. Anal. Bioanal. Chem. 408 (24), 6711–6717.